AGU ADVANCING EARTH AND SPACE SCIENCES

Geophysical Research Letters

RESEARCH LETTER
10.1029/2026GL122469

Does Geocentric Sea-Level Rise in the Maritime Continent Reveal a Tectonic Fingerprint?

Nidheesh Gangadharan[1,2], Sophie Coulson[3], Brent G. Delbridge[4], Grace Ertel[3], Aurel Moise[2], and Matthew D. Palmer[5,6]

[1]Indian National Centre for Ocean Information Services (INCOIS), Hyderabad, India, [2]Centre for Climate Research Singapore (CCRS), Singapore, Singapore, [3]Department of Earth Sciences, University of New Hampshire, Durham, NH, USA, [4]Earth and Environmental Sciences Division, Los Alamos National Laboratory, Los Alamos, NM, USA, [5]Met Office Hadley Centre, Exeter, UK, [6]School of Earth Sciences, University of Bristol, Bristol, UK

Key Points:

- A process decomposition of observed geocentric sea-level trends in the Maritime Continent is presented
- A residual signal emerges that coincides with GRACE-derived long-term geoid change along the 2004 Indian Ocean earthquake rupture zone
- This correspondence suggests a tectonic contribution to regional geocentric sea-level trends through gravity-field perturbations

Supporting Information:

Supporting Information may be found in the online version of this article.

Correspondence to:

N. Gangadharan,
nidheesh.ag@incois.gov.in

Citation:

Gangadharan, N., Coulson, S., Delbridge, B. G., Ertel, G., Moise, A., & Palmer, M. D. (2026). Does geocentric sea-level rise in the Maritime Continent reveal a tectonic fingerprint? *Geophysical Research Letters*, *53*, e2026GL122469. https://doi.org/10.1029/2026GL122469

Received 19 FEB 2026
Accepted 27 APR 2026

Author Contributions:

Conceptualization: Nidheesh Gangadharan
Formal analysis: Nidheesh Gangadharan, Sophie Coulson, Brent G. Delbridge, Grace Ertel
Investigation: Nidheesh Gangadharan, Sophie Coulson, Brent G. Delbridge
Methodology: Nidheesh Gangadharan, Sophie Coulson, Brent G. Delbridge, Grace Ertel
Project administration: Aurel Moise
Resources: Sophie Coulson
Supervision: Aurel Moise, Matthew D. Palmer
Visualization: Nidheesh Gangadharan
Writing – original draft: Nidheesh Gangadharan

Abstract The islands of the Maritime Continent are highly vulnerable to sea-level rise driven by barystatic, sterodynamic, and vertical land motion (VLM) processes. While tectonics is known to affect relative sea-level through VLM, its influence on long-term geocentric sea level (GSL) through crustal deformation and gravity field perturbations remains poorly constrained. A process decomposition of satellite-observed GSL change (1993–2021) reveals a significant residual trend along the Sumatra–Andaman subduction zone that cannot be explained by known oceanographic processes. This signal coincides with GRACE-derived long-term geoid change and the 2004 Indian Ocean earthquake rupture zone, indicating that tectonic deformation may imprint a measurable signal on long-term GSL change. Confirming this tectonic origin, given the possible deep ocean sterodynamic contributions, requires sustained ocean in situ observations and geophysical modeling.

Plain Language Summary The islands of Southeast Asia sit in one of the most tectonically active parts of the world, where earthquakes and crustal shifts can reshape the ocean floor. Sea level in this region is rising mainly due to ocean warming and melting of land ice, but the role of tectonics in these changes has been unclear. Using satellite sea-level measurements from 1993 to 2021, we separated sea-level rise into its main components and found an unusual pattern along the Sumatra-Andaman subduction zone that could not be explained by ocean or ice-related processes. This signal matches a slow change in Earth's gravity field near the site of the 2004 Indian Ocean earthquake. Our results suggest that long-term tectonic deformation may leave a fingerprint on sea-level change, independent of local land sinking or rising, providing a new way to understand how solid Earth processes influence the ocean surface.

1. Introduction

Coastal regions in the Maritime Continent (MC) are among the most vulnerable in the world to sea-level rise impacts, owing to climatic, non-climatic (e.g., land subsidence, dam impoundment), and socioeconomic (e.g., population density, adaptive capacity) factors (Nicholls et al., 2021). The region's complex oceanographic setting comprises shallow shelves, deep oceanic trenches, and narrow channels connecting the Pacific and the Indian Oceans. Consequently, accurately assessing and predicting the components of sea-level change across the region has historically been challenging (Feng et al., 2018; Meltzner et al., 2017; Wyrtki, 1961). The known processes that drive spatially variable geocentric sea-level (GSL) change (sea-level change with respect to the terrestrial reference frame) in the region are ocean sterodynamic sea-level (SDSL) changes (associated with changes in ocean density and circulation), the gravitational, rotational, and deformational (GRD) effects on sea level in response to contemporary mass redistribution (CMR) between the land and oceans (i.e., present land ice mass loss and terrestrial water storage [TWS] changes), and the glacial isostatic adjustment (GIA; Stammer et al., 2013; Hamlington et al., 2020; Wang et al., 2021).

The islands of the MC sit astride a complex network of active tectonic boundaries, including the Sumatra-Andaman subduction zone, which has hosted several of the largest earthquakes of the 21st century (Bilek & Lay, 2018; Shearer & Bürgmann, 2010). Both coseismic rupture and postseismic/interseismic deformation across the subduction zone directly contribute to vertical land motion (VLM), and displacements in the local density structure due to this deformation generate perturbations to Earth's gravity field, potentially significant enough to affect GSL (Broerse et al., 2014; Han et al., 2006; Melini et al., 2004; Panet et al., 2007). Though the impact of VLM on relative sea-level (RSL) change (i.e., sea-level change measured against a local datum fixed to land) in

Writing – review & editing: Nidheesh Gangadharan, Sophie Coulson, Brent G. Delbridge, Grace Ertel, Aurel Moise, Matthew D. Palmer

the region has been a subject of research (e.g., Peng et al., 2024; Tay et al., 2022), the role of tectonics modulating long-term GSL change remains elusive. A previous attempt to detect earthquake-driven long-term GSL change in the Indian Ocean pointed out the obscuring effect of dynamic sea-level variability (Tanaka et al., 2019). Here, we explore the relative roles of various physical processes in shaping sea-level rise observed in the MC during 1993–2021. Our GSL decomposition reveals a significant residual rate along the Sumatra-Andaman subduction region, suggesting a decadal modulation of GSL change by subduction tectonics.

2. Data and Method

2.1. Observations

We used monthly, gridded (0.25°), satellite sea-level anomalies (SLA; with respect to mean sea-surface height for the period 1993–2012) obtained from the Copernicus Climate Change Services (C3S; https://climate.copernicus.eu/), which is based on a merged product from multiple satellite missions (TOPEX/Poseidon, ERS-1/2, Jason-1, Jason-2, and Envisat), during 1993–2021. We also used monthly sea-level data from tide-gauge records obtained from the Permanent Service for Mean Sea Level (PSMSL) repository (Holgate et al., 2013; PSMSL, 2022). More details of the observed sea-level data are given in the Supporting Information S1 (Text S1). We used level-2 GRACE (The Gravity Recovery and Climate Experiment) gravity data from the Helmholtz Center for Geosciences (GFZ; Dahle et al., 2018) to estimate the surface geoid height in the region. The details of GRACE data processing and geoid computation are given in the Supporting Information S1 (Text S7).

2.2. Modeling the Processes Contributing to GSL Change

All sea-level terminology and concepts used in this study adhere to the definitions provided by J. M. Gregory et al. (2019). Barystatic and sterodynamic processes are the traditional mechanisms thought to drive regional sea surface height (SSH) change (the term "SSH" indicates a GSL change throughout the text, unless otherwise specified). Ocean circulation and density variations result in SDSL change, which is typically estimated from ocean models constrained to observations. Exchange of water mass between the oceans and land (e.g., land ice melting and variability in TWS) causes SSH changes, broadly termed barystatic sea-level change. As this mass moves across the Earth's surface, the associated GRD effects generate non-uniform spatiotemporal patterns of SSH change, often referred to as sea-level fingerprints (J. M. Gregory et al., 2019). Following Harvey et al. (2021), we term all SSH change driven by present mass exchange and associated GRD effects, CMR. We reserve the term GIA (Tamisiea & Mitrovica, 2011) for the ongoing impacts of the last ice age on SSH. Hence, the observed change in GSL can be decomposed and modeled as:

$$\text{GSL} = \text{SDSL} + \text{CMR (contemporary GRD effects)} + \text{GIA} + \text{Residual.} \quad (1)$$

The residual should contain contributions from unknown processes excluded in (1) and/or the error in the component estimations. We developed predictions for each process over the observational period (1993–2021) to examine whether the sum of contributions (on the right-hand side of [1]) can explain the observed GSL rate in the MC within the uncertainty levels.

In volume-conserving ocean models, SDSL is the sum of dynamic sea level (DSL) and global-mean thermosteric sea level (GMTSL). The salinity contribution (halosteric sea level) to global-mean sea level (GMSL) is practically zero (see Lowe & Gregory, 2006). Although freshwater from land is included in the ocean models in the form of river discharge, no GRD effects are present in these ocean models due to freshwater input. We considered SSH (after removing the GMSL) from four ocean reanalysis products: ORA-S5 (Zuo et al., 2019; covering 1993–2021), GECCO3 (Köhl, 2020, 1993–2018), GLORYS12V1 (Jean-Michel et al., 2021, 1993–2020), and SODA3 (Carton et al., 2018, 1993–2015) as our DSL. Even though each reanalysis product covers a different period, we constructed an ensemble mean of these four products so that our ensemble-mean SDSL covers the full period (1993–2021; Text S3 in Supporting Information S1). We estimated the GMTSL from ORAS-5 (Figure S3a in Supporting Information S1), and our GMTSL rate (1.2 mm yr^{-1}) is consistent with the observed GMTSL rate (Frederikse et al., 2020). We also computed the steric (sea-level change due to local density variations) and manometric (sea-level change associated with changes in ocean mass and bottom pressure) components of the SDSL change (Figures S4a and S4b in Supporting Information S1, respectively) as described in detail in Text S4 in Supporting Information S1. The ocean's internal mass redistribution also induces some GRD sea-level

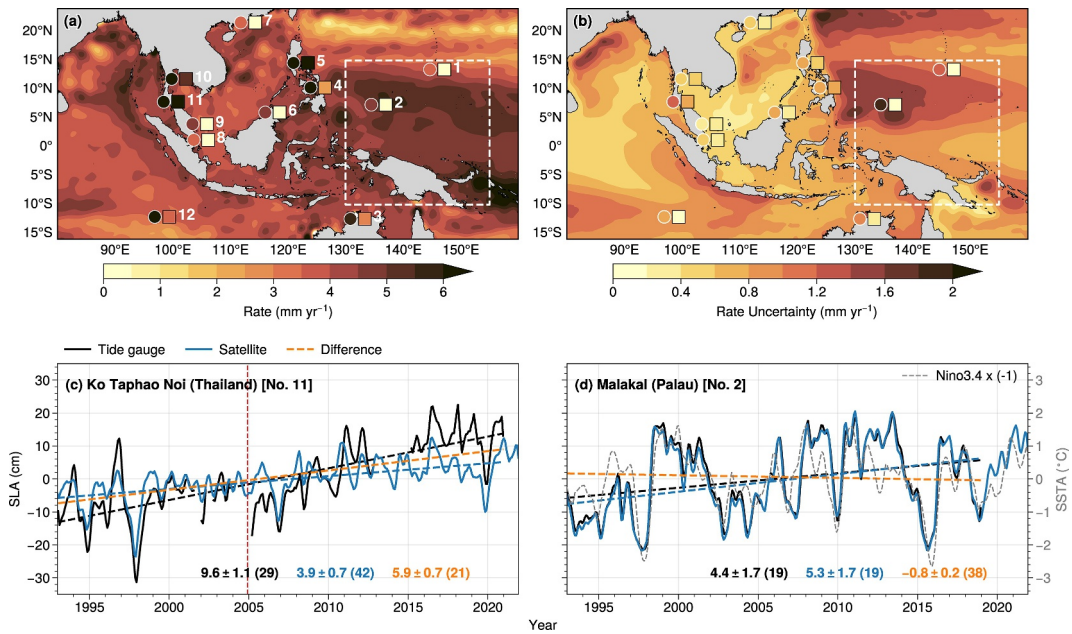

Figure 1. The observed sea-level rise in the Maritime Continent. (a) Rate of sea-level rise from satellite (spatial map) and tide-gauges (circles) for the period 1993–2021. The rate of residual signal (tide-gauge minus satellite time series averaged over a 1-degree circle around the tide-gauge location) is also shown (squares). (b) The sea-level trend uncertainty at 95% confidence level for satellite (spatial map), tide-gauges (circles), and difference time series (square). (c) Tide-gauge and satellite sea-level time series at Ko Taphao Noi (Thailand; location number 11 in panel (a)) and their linear trends (dashed lines). The linear trend line corresponding to the difference time series is also shown (orange). (d) Same as panel (c), but for the tide-gauge station at Malakal (Palau; location number 2 in panel (a)). The rate and uncertainty of sea level for satellite, tide-gauge, and difference signals are shown at the bottom of panels (c) and (d), with the corresponding colors (unit: mm/yr). The number in brackets indicates the effective sample size (methods) available for the respective time series. The vertical red line in panel c indicates the timing of the 2004 Indian Ocean earthquake. The Niño3.4 index (inverted) is shown in panel (d), indicating the climate control of low-frequency sea-level variations in the western Pacific.

response, especially in the shallow shelf regions, and those ocean GRD patterns are termed Self-Attraction and Loading (SAL; J. Gregory et al., 2013). We estimated the rate from SAL (Figure S4c in Supporting Information S1) using bottom pressure anomalies derived from manometric sea-level change (Text S4 in Supporting Information S1). We included this SAL-related GRD rate in our budget Equation 1, even though it is three orders of magnitude lower than the other terms. The computational details of these SDSL components are provided in Supporting Information S1 (Text S4).

To predict the GRD sea-level patterns of CMR between land ice (Antarctic and Greenland ice sheets and global glaciers), TWS, and the ocean, we solved the sea-level equation as described in Kendall et al. (2005) for each source individually, using recently published mass balance data sets for changes in land ice and TWS as input. The details of our GRD and GIA sea-level rate and uncertainty computations are provided in Supporting Information S1 (Text S5 and S6). Also, details of the rate-uncertainty computation for observed sea-level data (satellite and tide-gauge), SDSL (considering both temporal and product uncertainty), and the combined uncertainty of the predicted GSL rate are provided in Supporting Information S1 (Text S8).

3. Results

3.1. Observed Sea-Level Rise in the MC

Figure 1a shows the observed GSL and RSL (which includes VLM information) change across the region from satellite altimetry and tide-gauge data, respectively (associated uncertainties are given in Figure 1b). Mean sea level has been rising everywhere in the MC region since 1993, with a regional mean GSL rate of 4.1 mm yr^{-1}, higher than the GMSL rate over the same period (~3 mm yr^{-1}; without GIA correction). As calculating mean rates over the 1993–2021 period does not fully resolve low-frequency natural variability, some regions under the influence of strong climate modes exhibit notable rate deviations from the regional mean rate with higher

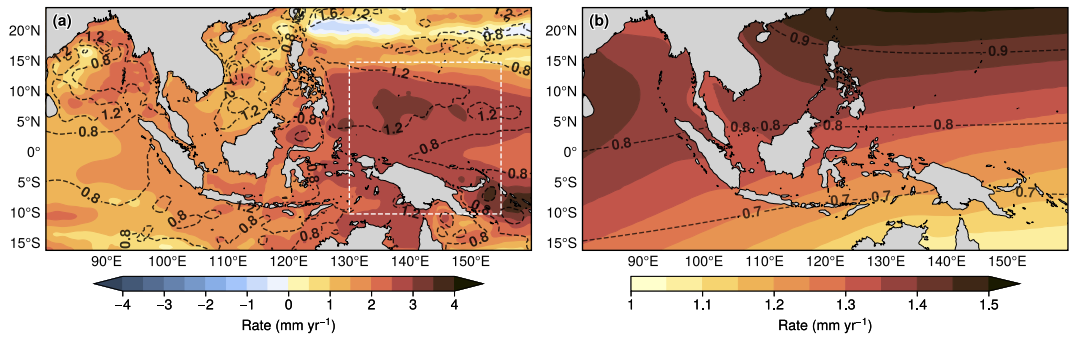

Figure 2. The sterodynamic and mass contributions. (a) Rate of sterodynamic sea-level (SDSL) change (color) and the rate uncertainty (contour) at 95% level (the uncertainty includes the product uncertainty as well [methods]). The western Pacific, where a larger SDSL change is observed, is highlighted (white rectangle, the same rectangle shown in Figure 1a). The SDSL time series averaged over the highlighted region is shown in Figure S4 in Supporting Information S1. The steric and manometric components of SDSL rate and the rate corresponding to ocean gravitational, rotational, and deformational effects (self-attraction and loading) are also shown in Figure S4 in Supporting Information S1. (b) (Color) The geocentric sea level rate of contemporary mass redistribution (CMR, i.e., sum of contributions from ice sheets, glaciers, and terrestrial water storages) and glacial isostatic adjustment and (contour) the associated uncertainty. The rate and uncertainty of CMR are provided in Figures S6 and S7 in Supporting Information S1, respectively.

uncertainties. The western tropical Pacific (region denoted by the dashed rectangle in Figure 1a), for instance, has a higher regional mean rate of ∼5 mm yr^{-1}, partly linked to decadal ENSO (El Niño-Southern Oscillation; Figure 1d). This study focuses on the origins of a region of significantly high GSL rates revealed by the satellite altimetry data in the eastern side of the North Indian Ocean (NIO) (Figure 1a) with minimal corresponding temporal uncertainty (Figure 1b).

A reasonable intercomparison between satellite and tide-gauge sea-level (given the correlation exceeds 0.6 for all selected tide-gauge records) provides confidence in attributing the rates from either source. Also, the difference in sea-level rates between tide-gauge and satellite records provides insight into long-term rates of local VLM (Wöppelmann & Marcos, 2016, Text S2 in Supporting Information S1). A visually evident shift in the Ko Taphao Noi record after 2005 (Thailand; location 11 in Figure 1a), for example, potentially demonstrates the coseismic and postseismic effect of the 2004 Sumatra earthquake on VLM (Figure 1c) and tide-gauge readings. While the effect of subduction zone seismicity on VLM and therefore tide-gauge time series has been the focus of several recent studies (Denys et al., 2020; Simons et al., 2019), the impact of earthquake activity on long-term GSL change has not been observationally constrained.

3.2. Processes Contributing to GSL Change

The western Pacific and northeast Bay of Bengal experienced higher rates of SDSL rise over the past decades (2–4 mm yr^{-1}; Figure 2a). The SDSL change in the western Pacific is closely linked to Pacific natural variability at interannual-to-decadal scales (e.g., Hamlington et al., 2013; Figure S4d in Supporting Information S1), leading to higher rate uncertainty as well (Figure 2a). An examination of steric and manometric components of the SDSL shows that the steric sea-level rise contributes to the SDSL rise mainly over deep oceans, while the manometric change is prominent over shallow shelf regions in the MC (Figures S4a and S4b in Supporting Information S1). Loading into the shallow shelves in response to a deep-to-shallow steric sea-level gradient (e.g., Landerer et al., 2007; Figure S4a in Supporting Information S1) can induce some GRD effects via SAL, thereby further affecting sea level. However, the SAL rate is a few orders of magnitude smaller than other contributions, yet it reaches a maximum in the shallow Sunda region (Figure S4c in Supporting Information S1). The net SDSL uncertainty in the South China Sea (SCS) is comparatively large, partly due to higher product uncertainty (Figure S3c and Text S8 in Supporting Information S1). Note that the net SDSL uncertainty is minimal in the eastern Indian Ocean, where this study is focused.

The GRD and GIA rates in the MC are relatively spatially uniform compared to dynamic sea-level rates (Figures S5–S7 in Supporting Information S1) or GRD rates observed over higher latitudes (e.g., Coulson et al., 2022), indicating that the non-uniform spatial patterns in the observed GSL rise (Figure 1a) arise mainly from SDSL change (Figure 2a). The combined GSL rate of CMR and GIA varies between 1–1.5 mm yr^{-1}, as shown in

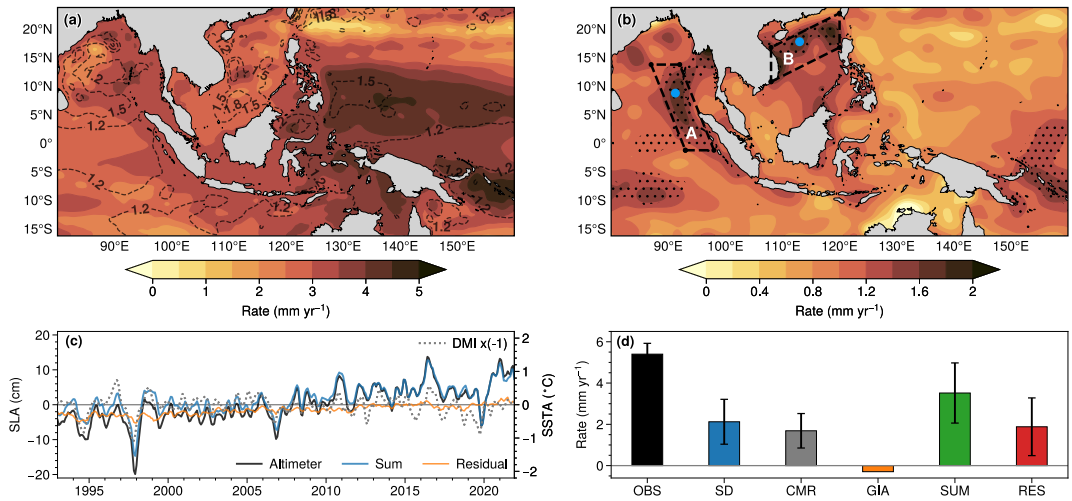

Figure 3. The predicted and residual sea-level rates. (a) (Color) The predicted total geocentric sea level rate (i.e., the sum of sterodynamic sea-level, self-attraction and loading, CMR, and GIA) and (contour) the corresponding rate uncertainty. (b) (Color) The residual sea-level (i.e., altimeter-sum) rate and the black dots represent grids where the residual rate is larger than the net uncertainty. The eastern North Indian Ocean (A) and northern South China Sea (B), where significant residual rates were observed, are shown by parallelograms in panel (b). The blue dots in these two regions indicate the grid points at which sea-level time series are extracted and shown in Figure S9 in Supporting Information S1. (c) The spatial mean (averaged over the parallelogram A) sea-level time series from the altimeter (black; rate = 4.65 ± 0.5 mm yr^{-1}), sum of contributions (blue; rate = 3.18 ± 0.45 mm yr^{-1}), and their difference time series (orange; rate = 1.47 ± 0.12 mm yr^{-1}). The dipole mode index is also overlaid (multiplied by −1). (d) The observed and the contributing rates extracted at a grid point in the eastern Indian Ocean (shown by blue dot in parallelogram A) where maximum residual rate is observed, along with corresponding uncertainties: SD (sterodynamic), CMR (contemporary mass redistribution), GIA (glacial isostatic adjustment), SUM (sum of contributions), and RES (residual rate).

Figure 2b. Figure 3a presents the predicted GSL rate (sum of contributions) and total uncertainty. The pattern of the predicted rate generally aligns with the observed altimetry rate (Figure 1a), although a clear underestimation persists throughout the region. The residual rate (observed–predicted) is positive everywhere and ranges between 0 and 2 mm yr^{-1} (Figure 3b). Note that a 3 × 3° spatial filter is applied to the original residual rate (shown in Figure S8 in Supporting Information S1) following the method of Grooms et al. (2021) to discard mesoscale, eddy-like noise. The agreement varies regionally; for instance, the predicted rate in the western Pacific is close to the observed rate (~4–5 mm yr^{-1}), and the residual rates are confined within the uncertainty bounds (less than 0.5 mm yr^{-1}) in this region. The discrepancies are higher toward the west, especially in the northern SCS and the eastern side of the NIO, as highlighted by parallelograms labeled B and A, respectively, in Figure 3b.

To address the role of climate variability in affecting GSL rates in the NIO region, as suggested by Tanaka et al. (2019), we compared the dipole mode index (DMI), representing the Indian Ocean Dipole (IOD) with the predicted sea-level time series (sum of contributions) in the NIO (Figure 3c). The model sea level and DMI correlate moderately ($r = -0.6$), showing influence of IOD on sea-level variability in this region. Nevertheless, the (detrended) observed and predicted sea-level in the NIO (Figure 3c) highly correlate with each other ($r = 0.95$), assuring that we effectively remove such climate-driven, low-frequency ocean signals through our reanalysis-based sterodynamic variability. But we have the following observations for low-frequency sea-level variability in the SCS region:

1. The SCS is one of the least sampled marginal seas in the past (e.g., Nidheesh et al., 2017), and therefore, the reanalysis systems are poorly constrained by observed changes in this region. As shown in Figure S3c in Supporting Information S1, there is a large "product uncertainty" for dynamic sea-level change in the SCS, but that is relatively smaller in the NIO.
2. The sterodynamic rates in the SCS may also potentially be affected by strong (chaotic) internal variability, as shown in Llovel et al. (2018). Altimeter and sterodynamic time series extracted at a point in the SCS (blue dot in Figure 3b) exhibit a weak cross-correlation (0.71), suggesting such locally driven internal variability (Figure S9b in Supporting Information S1). Constraining such variability remains a challenge for reanalysis systems

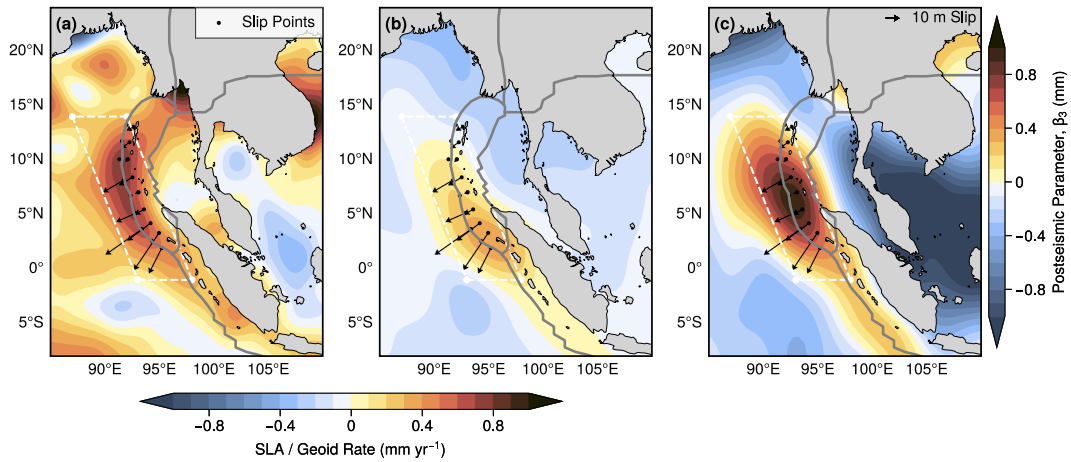

Figure 4. The residual sea-level and GRACE-derived geoid change fields in the eastern Indian Ocean. (a) (Color) The residual sea-level rate over the eastern Indian Ocean for 1993–2021. (b) (Color) GRACE-derived geoid rate for 2002–2017. Both fields in panels (a) and (b) are shown after removal of the regional mean over the Maritime Continent (see Main Text). (c) Fitted magnitude of the postseismic logarithmic term from the event-based GRACE geoid regression model (Text S7 in Supporting Information S1), representing the strength of postseismic response (mm). In all panels, gray curves denote plate boundaries from Bird (2003). Arrow vectors show the best-fit slip model for the 2004 Sumatra-Andaman earthquake on 18 subfault patches, obtained by joint inversion of tsunami and geodetic data from Lorito et al. (2010). The white dashed parallelogram marks the region where the maximum residual SLA rates are observed. Note, panels (a) and (b) use the bottom color scale, and panel (c) uses the color scale shown to the right.

due to the sparse resolution of ocean models and the limited availability of observational data. On the other hand, the altimeter and sterodynamic time series extracted in the NIO (blue dot in Figure 3b) exhibit a strong cross-correlation (0.92), indicating that the reanalysis products effectively capture oceanic variability in this region (Figure S9a in Supporting Information S1).

Based on these combined considerations, we restrict our focus and interpretation of a potential tectonic contribution to the SSH residual rate in the Sumatra region and do not extend this hypothesis to the SCS.

3.3. Residual GSL Rate and Connection With Active Tectonics

Our budget analysis of the regional GSL change in the NIO, as summarized in Figures 3c and 3d, suggests that the residual SLA rate exceeds the "net uncertainty" (see Text S8 in Supporting Information S1) in the NIO (region A; Figure 3b), indicating that additional processes must be contributing to the observed rate. To isolate anomalous regional residual rates in region A beyond this uncertainty, we subtracted the spatially averaged residual rate in the MC (~1 mm yr^{-1}) from the original residual field.

The anomalous residual SLA rate exhibits a high along the Sumatra-Andaman subduction zone (Figure 4a; plate boundaries from Bird (2003) are plotted as gray lines). Both coseismic rupture and postseismic deformation are known to generate gravity highs and lows in the region of deformation through vertical displacements of density interfaces and volumetric density changes, which are detectable in GRACE gravity data (Han et al., 2006; Panet et al., 2007; Pollitz et al., 2006). Postseismic relaxation occurs through a combination of processes such as mantle creep and localized afterslip, which can produce long-term gravity trends. In addition, ongoing seismic and aseismic activity along the subduction zone may also contribute to the observed gravity field, making it difficult to attribute the GRACE signal to any single process associated with the 2004 Indian Ocean earthquake (Broerse et al., 2015). Nevertheless, the combined long-term gravity changes from these processes are expected to perturb the equilibrium SSH.

Figure 4b shows the rate of geoid height change inferred from GRACE during the 2002–2017 period. The mean geoid height across the MC region is subtracted to remove the influence of any long-wavelength signal, and to facilitate comparison with the anomalous residual SLA rate. Following Tamisiea (2011) and Adhikari et al. (2019), because the equilibrium sea surface follows the geoid, any local perturbation in geoid height is expected to produce a corresponding perturbation in SSH. However, the mean SSH and mean geoid need not

match, since the ocean surface can shift relative to the geoid when mass is redistributed, and because reference-frame changes may alter the global offset (Dahlen, 1976). This discrepancy is likely reduced by removing the spatial mean from both residual sea level and geoid. Therefore, the spatial pattern of geoid height perturbation (Figure 4b) can be interpreted as analogous to a time-averaged change in GSL over the region due to mass redistribution, with a significant contribution likely arising from tectonic processes (Álvarez et al., 2021; Zhu et al., 2023).

The maximum change in geoid height is observed along the Sumatra-Andaman subduction zone, with peak values near the region of maximum slip during the 2004 Sumatra earthquake (the best-fit slip model from Lorito et al. (2010) is shown as arrow vectors). The spatial structure of the geoid rate highs along the subduction zone (Figure 4b) broadly aligns with the pattern of residual GSL rates (Figure 4a), though the maximum rates are further south in the geoid rates. The anomalous residual rate examined here is based on processed monthly SLA rather than absolute SSH; therefore, it may not capture abrupt, step-like changes, such as coseismic geoid shifts associated with rapid deformation. As a result, the residual SLA (Figure 3c) is not expected to robustly resolve a coseismic signal, even if such a signal is present in absolute SSH or GRACE-derived gravity change. By contrast, the long-term residual rate is more likely to reflect the slowly evolving component associated with postseismic deformation.

To isolate the longer-lived postseismic signal in the GRACE record, we additionally fit the GRACE geoid time series using an event-based regression model that includes seasonal variability, a coseismic step, and a logarithmic postseismic relaxation term referenced to the 2004 earthquake (Text S7 in Supporting Information S1). The fitted magnitude of the postseismic term is shown in Figure 4c. This field more directly isolates the long-term postseismic component than the period-mean geoid-rate shown in Figure 4b, and it exhibits a spatial pattern broadly consistent with the residual SLA rate signal along the trench. Quantitative differences between the GRACE geoid rate and the residual GSL rate are expected. The altimeter SLA rate may be influenced by unresolved ocean decadal variability in the region (e.g., Tanaka et al., 2019), whereas the GRACE geoid-based fields are less sensitive to such variability. Additional differences may also arise because the GRACE and altimeter records do not span the same periods. Nevertheless, the spatial correspondence between the residual SLA rate and both the GRACE geoid-rate and the postseismic response fields, despite these quantitative differences, provides supporting evidence that tectonic deformation contributes to the observed residual GSL rate in the region.

4. Conclusions

Both coseismic and postseismic deformation in subduction zones perturb the local gravity field, a response well documented in gravimetry data sets (e.g., Broerse et al., 2015; Han et al., 2008). Given that equilibrium SSH lies on a gravitational equipotential, tectonic gravity perturbations are expected to influence SSH (Broerse et al., 2014; Melini et al., 2004); however, these tectonically-driven signals have been challenging to disentangle from the suite of processes contributing to local variations in GSL, particularly ocean dynamic variability (Tanaka et al., 2019). By carefully decomposing satellite-observed GSL into its known components, we identify an anomalous residual GSL rate along the Sumatra-Andaman subduction zone that shows spatial correspondence with the subduction trench geometry, the 2004 earthquake coseismic slip distribution, and GRACE-derived geoid perturbations associated with postseismic deformation. Long-term geoid-height anomalies observed by GRACE exhibit similar geometries and provide supporting evidence that tectonic deformation contributes to SSH changes that persist beyond the coseismic rupture period, potentially introducing decadal-scale perturbations to SSH. Although ocean observations have improved substantially over the past few decades, sampling of the deep ocean, especially below 2000 m, remains limited. Better constraining the relative roles of tectonic deformation and low-frequency ocean variability in the observed SLA rate in the eastern Indian Ocean will therefore require sustained in situ ocean observations together with postseismic geodetic modeling.

Conflict of Interest

The authors declare no conflicts of interest relevant to this study.

Availability Statement

All observational and reanalysis data used in this study are publicly available. The gridded altimeter sea-level data are provided by the Copernicus Climate Change Service (2021; https://doi.org/10.48670/moi-00145), and ERA-5 sea-level pressure data are obtained from the Copernicus Climate Change Service (2023; https://doi.org/10.24381/cds.f17050d7). The data sets generated and analyzed in this study are available at Zenodo (Gangadharan, 2026) and can be accessed via https://doi.org/10.5281/zenodo.19955186.

Acknowledgments
N.G. acknowledges the research facilities provided by ESSO-INCOIS, Hyderabad, Ministry of Earth Sciences (MoES), India. M.D.P. was supported by the Met Office Hadley Centre Climate Programme, funded by DSIT. G.E. was supported by the University of New Hampshire Department of Earth Sciences. We acknowledge ProPlot (https://proplot.readthedocs.io/en/latest/#) for preparing the figures. We thank the two anonymous reviewers for their constructive comments, which improved the manuscript. This is INCOIS contribution number – 711.

References

Adhikari, S., Ivins, E. R., Frederikse, T., Landerer, F. W., & Caron, L. (2019). Sea-level fingerprints emergent from GRACE mission data. *Earth System Science Data*, *11*(2), 629–646. https://doi.org/10.5194/essd-11-629-2019

Álvarez, O., Pechuan Canet, S., Gimenez, M., & Folguera, A. (2021). Megathrust slip behavior for great earthquakes along the Sumatra–Andaman subduction zone mapped from satellite GOCE gravity field derivatives. *Frontiers in Earth Science*, *8*, 581396. https://doi.org/10.3389/feart.2020.581396

Bilek, S. L., & Lay, T. (2018). Subduction zone megathrust earthquakes. *Geosphere*, *14*(4), 1468–1500. https://doi.org/10.1130/ges01608.1

Bird, P. (2003). An updated digital model of plate boundaries. *Geochemistry, Geophysics, Geosystems*, *4*(3), 1027. https://doi.org/10.1029/2001GC000252

Broerse, T., Riva, R., Simons, W., Govers, R., & Vermeersen, B. (2015). Postseismic GRACE and GPS observations indicate a rheology contrast above and below the Sumatra slab. *Journal of Geophysical Research: Solid Earth*, *120*(7), 5343–5361. https://doi.org/10.1002/2015JB011951

Broerse, T., Riva, R., & Vermeersen, B. (2014). Ocean contribution to seismic gravity changes: The sea level equation for seismic perturbations revisited. *Geophysical Journal International*, *199*(2), 1094–1109. https://doi.org/10.1093/gji/ggu315

Carton, J. A., Chepurin, G. A., & Chen, L. (2018). SODA3: A new ocean climate reanalysis. *Journal of Climate*, *31*(17), 6967–6983. https://doi.org/10.1175/JCLI-D-18-0149.1

Copernicus Climate Change Service. (2021). Global ocean gridded L4 sea surface heights and derived variables reprocessed (Copernicus Climate Change Service) [Dataset]. *Mercator Ocean International*. https://doi.org/10.48670/MOI-00145

Copernicus Climate Change Service. (2023). ERA5 monthly averaged data on single levels from 1940 to the present [Dataset]. *Copernicus Climate Change Service (C3S) Climate Data Store (CDS)*. https://doi.org/10.24381/cds.f17050d7

Coulson, S., Dangendorf, S., Mitrovica, J. X., Tamisiea, M. E., Pan, L., & Sandwell, D. T. (2022). A detection of the sea level fingerprint of Greenland Ice Sheet melt. *Science*, *377*(6614), 1550–1554. https://doi.org/10.1126/science.abo0926

Dahle, C., Flechtner, F., Murböck, M., Michalak, G., Neumayer, H., Abrykosov, O., et al. (2018). GRACE geopotential GSM coefficients GFZ RL06 (Version 6.0) [Dataset]. *GFZ Data Services*. https://doi.org/10.5880/GFZ.GRACE_06_GSM

Dahlen, F. A. (1976). The passive influence of the oceans upon the rotation of the Earth. *Geophysical Journal of the Royal Astronomical Society*, *46*(2), 363–406. https://doi.org/10.1111/j.1365-246x.1976.tb04163.x

Denys, P. H., Beavan, R. J., Hannah, J., Pearson, C. F., Palmer, N., Denham, M., & Hreinsdottir, S. (2020). Sea level rise in New Zealand: The effect of vertical land motion on century-long tide gauge records in a tectonically active region. *Journal of Geophysical Research: Solid Earth*, *125*(1), e2019JB018055. https://doi.org/10.1029/2019jb018055

Feng, M., Biastoch, A., Benthuysen, J., Wijffels, T. W., & McPhaden, S. (2018). The Indonesian throughflow, its variability and centennial change. *Geoscience Letters*, *5*(1), 3. https://doi.org/10.1186/s40562-018-0102-2

Frederikse, T., Landerer, F., Caron, L., Adhikari, S., Parkes, D., Humphrey, V. W., et al. (2020). The causes of sea-level rise since 1900. *Nature*, *584*(7821), 393–397. https://doi.org/10.1038/s41586-020-2591-3

Gangadharan, N. (2026). Does geocentric sea-level rise in the Maritime Continent reveal a tectonic fingerprint? *Zenodo* [Dataset]. https://doi.org/10.5281/zenodo.19955186

Gregory, J., White, N., Church, J., Bierkens, M., Box, J., van den Broeke, R., et al. (2013). Twentieth-century global-mean sea-level rise: Is the whole greater than the sum of the parts? *Journal of Climate*, *26*(13), 4476–4499. https://doi.org/10.1175/JCLI-D-12-00319.1

Gregory, J. M., Griffies, S. M., Hughes, C. W., Lowe, J. A., Church, J. A., Fukimori, I., et al. (2019). Concepts and terminology for sea level: Mean, variability and change, both local and global. *Surveys in Geophysics*, *40*(6), 1251–1289. https://doi.org/10.1007/s10712-019-09525-z

Grooms, I., Loose, N., Abernathey, R., Steinberg, J. M., Bachman, S. D., Marques, G., et al. (2021). Diffusion-based smoothers for spatial filtering of gridded geophysical data. *Journal of Advances in Modeling Earth Systems*, *13*(9), e2021MS002552. https://doi.org/10.1029/2021MS002552

Hamlington, B. D., Gardner, A. S., Ivins, E., Lenaerts, J. T. M., Reager, J. T., Trossman, D. S., et al. (2020). Understanding of contemporary regional sea-level change and the implications for the future. *Reviews of Geophysics*, *58*(3), e2019RG000672. https://doi.org/10.1029/2019rg000672

Hamlington, B. D., Leben, R. R., Strassburg, M. W., Nerem, R. S., & Kim, K. Y. (2013). Contribution of the Pacific Decadal Oscillation to global mean sea level trends. *Geophysical Research Letters*, *40*(19), 5171–5175. https://doi.org/10.1002/grl.50950

Han, S.-C., Sauber, J., Luthcke, S. B., Ji, C., & Pollitz, F. F. (2008). Implications of postseismic gravity change following the great 2004 Sumatra–Andaman earthquake from the regional harmonic analysis of GRACE intersatellite tracking data. *Journal of Geophysical Research*, *113*(B11), B11413. https://doi.org/10.1029/2008jb005705

Han, S.-C., Shum, C. K., Bevis, M., Ji, C., & Kuo, C. Y. (2006). Crustal dilatation observed by GRACE after the 2004 Sumatra–Andaman earthquake. *Science*, *313*(5787), 658–662. https://doi.org/10.1126/science.1128661

Harvey, T. C., Hamlington, B. D., Frederikse, T., Nerem, R. S., Piecuch, C. G., Hammond, W. C., et al. (2021). Ocean mass, sterodynamic effects, and vertical land motion largely explain US coast relative sea level rise. *Communications Earth & Environment*, *2*(1), 233. https://doi.org/10.1038/s43247-021-00300-w

Holgate, S. J., Matthews, A., Woodworth, P. L., Rickards, L. J., Tamisiea, M. E., Bradshaw, E., et al. (2013). New data systems and products at the Permanent Service for Mean Sea Level. *Journal of Coastal Research*, *29*(3), 493–504. https://doi.org/10.2112/JCOASTRES-D-12-00175.1

Jean-Michel, L., Eric, G., Romain, B. B., Gilles, G., Angélique, M., Marie, D., et al. (2021). The copernicus global 1/12° Oceanic and sea ice GLORYS12 reanalysis. *Frontiers in Earth Science*, *9*, 698876. https://doi.org/10.3389/feart.2021.698876

Kendall, R. A., Mitrovica, J. X., & Milne, G. A. (2005). On post-glacial sea level–II. Numerical formulation and comparative results on spherically symmetric models. *Geophysical Journal International*, *161*(3), 679–706. https://doi.org/10.1111/j.1365-246x.2005.02553.x

Köhl, A. (2020). Evaluating the GECCO3 1948–2018 ocean synthesis – A configuration for initializing the MPI-ESM climate model. *Quarterly Journal of the Royal Meteorological Society*, *146*(730), 2250–2273. https://doi.org/10.1002/qj.3790

Landerer, F. W., Jungclaus, J. H., & Marotzke, J. (2007). Regional dynamic and steric sea level change in response to the IPCC-A1B scenario. *Journal of Physical Oceanography*, *37*(2), 296–312. https://doi.org/10.1175/JPO3013.1

Llovel, W., Penduff, T., Meyssignac, B., Molines, J., Terray, L., Bessières, L., & Barnier, B. (2018). Contributions of atmospheric forcing and chaotic ocean variability to regional sea level trends over 1993–2015. *Geophysical Research Letters*, *45*(24), 13405–13413. https://doi.org/10.1029/2018GL080838

Lorito, S., Piatanesi, A., Cannelli, V., Romano, F., & Melini, D. (2010). Kinematics and source zone properties of the 2004 Sumatra–Andaman earthquake and tsunami: Nonlinear joint inversion of tide gauge, satellite altimetry, and GPS data. *Journal of Geophysical Research*, *115*(B2), B02304. https://doi.org/10.1029/2008jb005974

Lowe, J. A., & Gregory, J. M. (2006). Understanding projections of sea level rise in a Hadley Centre coupled climate model. *Journal of Geophysical Research*, *111*(C11), C11014. https://doi.org/10.1029/2005JC003421

Melini, D., Piersanti, A., Spada, G., Soldati, G., Casarotti, E., & Boschi, E. (2004). Earthquakes and relative sea level changes. *Geophysical Research Letters*, *31*(9), L09605. https://doi.org/10.1029/2003gl019347

Meltzner, A. J., Horton, B. P., Cheng, H., Zong, K. Y., Edwards, R. L., Hill, D. F., et al. (2017). Half-metre sea-level fluctuations on centennial timescales from mid-Holocene corals of Southeast Asia. *Nature Communications*, *8*(1), 14387. https://doi.org/10.1038/ncomms14387

Nicholls, R. J., Kopp, R. E., Small, C. S. P. G., Holgate, S. J., Kelley, J. J. W., Little, A. W., et al. (2021). A global analysis of subsidence, relative sea-level change and coastal flood exposure. *Nature Climate Change*, *11*(4), 338–342. https://doi.org/10.1038/s41558-021-00993-z

Nidheesh, A. G., Lengaigne, M., Vialard, J., Izumo, T., Unnikrishnan, A. S., Meyssignac, B., et al. (2017). Robustness of observation-based decadal sea level variability in the Indo-Pacific Ocean. *Geophysical Research Letters*, *44*(14), 7391–7400. https://doi.org/10.1002/2017gl073955

Panet, I., Mikhailov, V., Diament, M., Pollitz, F., King, G., de Viron, O., et al. (2007). Coseismic and post-seismic signatures of the Sumatra 2004 December and 2005 March earthquakes in GRACE satellite gravity. *Geophysical Journal International*, *171*(1), 177–190. https://doi.org/10.1111/j.1365-246x.2007.03525.x

Peng, D., Ng, G., Feng, L., Cazenave, A., & Hill, E. M. (2024). Coastal vertical land motion across Southeast Asia derived from combining tide gauge and satellite altimetry observations. *Science of Remote Sensing*, *10*, 100176. https://doi.org/10.1016/j.srs.2024.100176

Permanent Service for Mean Sea Level, PSMSL. (2022). Tide gauge data. Retrieved from http://www.psmsl.org/data/obtaining/

Pollitz, F. F., Bürgmann, R., & Banerjee, P. (2006). Post-seismic relaxation following the great 2004 Sumatra–Andaman earthquake on a compressible self-gravitating Earth. *Geophysical Journal International*, *167*(1), 397–420. https://doi.org/10.1111/j.1365-246x.2006.03018.x

Shearer, P. M., & Bürgmann, R. (2010). Lessons learned from the 2004 Sumatra-Andaman megathrust rupture. *Annual Review of Earth and Planetary Sciences*, *38*(1), 103–131. https://doi.org/10.1146/annurev-earth-040809-152537

Simons, W. J. F., Naeije, M. C., Brown, B. E., Niemnil, S., Pradit, S., Thongtham, N., et al. (2019). Vertical motion of Phuket Island (1994–2018) due to the Sumatra–Andaman mega-thrust earthquake cycle: Impact on sea-level and consequences for coral reefs. *Marine Geology*, *414*, 92–102. https://doi.org/10.1016/j.margeo.2019.05.008

Stammer, D., Cazenave, A., Ponte, R. M., & Tamisiea, M. E. (2013). Causes for contemporary regional sea level changes. *Annual Review of Marine Science*, *5*(1), 21–46. https://doi.org/10.1146/annurev-marine-121211-172406

Tamisiea, M. E. (2011). Ongoing glacial isostatic contributions to observations of sea level change. *Geophysical Journal International*, *186*(3), 1036–1044. https://doi.org/10.1111/j.1365-246x.2011.05116.x

Tamisiea, M. E., & Mitrovica, J. X. (2011). The moving boundaries of sea level change: Understanding the origins of geographic variability. *Oceanography*, *24*(2), 24–39. https://doi.org/10.5670/oceanog.2011.25

Tanaka, Y., Yu, Y., & Chao, B. F. (2019). Gravity and geoid changes by the 2004 and 2012 Sumatra earthquakes from satellite gravimetry and ocean altimetry. *Terrestrial, Atmospheric and Oceanic Sciences*, *30*(4), 531–540. https://doi.org/10.3319/TAO.2018.10.24.02

Tay, C., Lindsey, E. O., Chin, S. T., McCaughey, J. W., Bekaert, D., Nguyen, M., et al. (2022). Sea-level rise from land subsidence in major coastal cities. *Nature Sustainability*, *5*(12), 1049–1057. https://doi.org/10.1038/s41893-022-00947-z

Wang, J., Church, J. A., Zhang, X., Gregory, J. M., Zanna, L., & Chen, X. (2021). Evaluation of the local sea-level budget at tide gauges since 1958. *Geophysical Research Letters*, *48*(20), e2021GL094502. https://doi.org/10.1029/2021GL094502

Wöppelmann, G., & Marcos, M. (2016). Vertical land motion as a key to understanding sea level change and variability. *Reviews of Geophysics*, *54*(1), 64–92. https://doi.org/10.1002/2015RG000502

Wyrtki, K. (1961). *Physical oceanography of the Southeast Asian waters* (2nd ed.). NAGA Report, Scripps Institution of Oceanography. https://doi.org/10.1017/S0025315400054370

Zhu, F., Liu, X., Li, Z., Yuan, J., Guo, J., & Sun, H. (2023). High spatial resolution marine gravity trend determined from multisatellite altimeter data over Bay of Bengal. *Geophysical Journal International*, *235*(3), 2257–2267. https://doi.org/10.1093/gji/ggad368

Zuo, H., Alonso-Balmaseda, M., Mogensen, E., Mayer, M., & Tietsche, S. (2019). The ECMWF operational ensemble reanalysis–analysis system for ocean and sea ice: A description of the system and assessment. *Ocean Science*, *15*(3), 779–808. https://doi.org/10.5194/os-15-779-2019

References From the Supporting Information

Blewitt, G. (2003). Self-consistency in reference frames, geocenter definition, and surface loading of the solid Earth. *Journal of Geophysical Research*, *108*, 2103. https://doi.org/10.1029/2002jb002082

Dziewonski, A. M., & Anderson, D. L. (1981). Preliminary reference Earth model. *Physics of the Earth and Planetary Interiors*, *25*(4), 297–356. https://doi.org/10.1016/0031-9201(81)90046-7

Gravelle, M., Becker, M., Collilieux, X., Altamimi, Z., Wöppelmann, G., Testut, L., et al. (2023). The ULR-repro3 GPS data reanalysis and its estimates of vertical land motion at tide gauges for sea level science. *Earth System Science Data*, *15*(1), 497–509. https://doi.org/10.5194/essd-15-497-2023

Hersbach, H., Bell, B., Berrisford, P., Hirahara, S., Horányi, A., Muñoz-Sabater, J., et al. (2020). The ERA5 global reanalysis. *Quarterly Journal of the Royal Meteorological Society*, *146*(730), 1999–2049. https://doi.org/10.1002/qj.3803

Jackett, D. R., & McDougall, T. J. (1995). Minimal adjustment of hydrographic profiles to achieve static stability. *Journal of Atmospheric and Oceanic Technology*, *12*(2), 381–389. https://doi.org/10.1175/1520-0426(1995)012<0381:MAOHPT>2.0.CO;2

Jekeli, C. (1981). *Alternative methods to smooth the Earth's gravity field*. Rep. 327. Ohio State University Press.

Leith, C. E. (1973). The standard error of time-averaged estimates of climatic means. *Journal of Applied Meteorology*, *12*(6), 1066–1069. https://doi.org/10.1175/1520-0450(1973)012<1066:TSEOTA>2.0.CO;2

Loomis, B. D., Rachlin, K. E., Wiese, D. N., Landerer, F. W., & Luthcke, S. B. (2020). Replacing GRACE/GRACE-FO with satellite laser ranging: Impacts on Antarctic Ice Sheet mass change. *Geophysical Research Letters*, *47*, e2019GL085488. https://doi.org/10.1029/2019GL085488

Malles, J.-H., & Marzeion, B. (2021). Twentieth century global glacier mass change: An ensemble-based model reconstruction. *The Cryosphere*, *15*(7), 3135–3157. https://doi.org/10.5194/tc-15-3135-2021

Nilsson, J., Gardner, A., & Paolo, F. (2021). Elevation change of the Antarctic Ice Sheet: 1985 to 2020. *Earth System Science Data Discussions*, 1–39. https://doi.org/10.5194/essd-2021-305

Peltier, W. R., Argus, D. F., & Drummond, R. (2015). Space geodesy constrains ice-age terminal deglaciation: The global ICE-6G_C (VM5a) model. *Journal of Geophysical Research: Solid Earth*, *120*(1), 450–487. https://doi.org/10.1002/2014JB011176

Richter, K., Riva, R. E. M., & Drange, H. (2013). Impact of self-attraction and loading effects induced by shelf mass loading on projected regional sea level rise. *Geophysical Research Letters*, *40*(6), 1144–1148. https://doi.org/10.1002/grl.50265

Simonsen, S. B., Sørensen, A., Forsberg, R., Bamber, J. L., Csatho, B., Price, S. F., & Willis, M. J. (2021). Greenland Ice Sheet mass balance (1992–2020) from calibrated radar altimetry. *Geophysical Research Letters*, *48*, e2020GL091216. https://doi.org/10.1029/2020GL091216

Sutterley, T. C., & Velicogna, I. (2019). Improved estimates of geocenter variability from time-variable gravity and ocean model outputs. *Remote Sensing*, *11*(18), 2108. https://doi.org/10.3390/rs11182108

Swenson, S., & Wahr, J. (2006). Post-processing removal of correlated errors in GRACE data. *Geophysical Research Letters*, *33*(8), L08402. https://doi.org/10.1029/2005GL025285

Yin, J., Wang, T., Chen, X., Yu, L., Liu, P., Li, F., et al. (2023). GTWS-MLrec: Global terrestrial water storage reconstruction by machine learning from 1940 to present. *Earth System Science Data*, *15*(12), 5597–5615. https://doi.org/10.5194/essd-15-5597-2023